Nuclear magnetic resonance polarization and coherence echoes in static and rotating solids

M. Tomaselli[a)]
Laboratorium für Physikalische Chemie and Institut für Polymere, Eidgenössische Technische Hochschule, CH-8092 Zürich, Switzerland

S. Hediger
Laboratorium für Physikalische Chemie, Eidgenössische Technische Hochschule, CH-8092 Zürich, Switzerland

D. Suter
Fachbereich Physik, Universität Dortmund, D-44221 Dortmund, Germany

R. R. Ernst
Laboratorium für Physikalische Chemie, Eidgenössische Technische Hochschule, CH-8092 Zürich, Switzerland

(Received 1 February 1996; accepted 19 September 1996)

The mechanisms of defocusing and refocusing of spin order in extended dipolar coupled nuclear spin systems are investigated by experiments on static and on rotating solids. It is demonstrated that polarization or coherence echoes are possible also under magic-angle sample spinning. The dipolar interactions, averaged by the spinning, are recovered by rotor-synchronized multiple-pulse sequences. By a simple modification of the pulse sequences, it is possible to reverse the sign of the effective dipolar Hamiltonian and to induce the refocusing of polarization or coherence. The creation of multiple-spin order in the course of polarization evolution or free precession is monitored by a modified echo experiment. Experimental results for a polycrystalline sample of calcium formate are presented. © *1996 American Institute of Physics.* [S0021-9606(96)01148-8]

I. INTRODUCTION

Despite the fact that a closed system of interacting spins can be described by a deterministic quantum-mechanical equation of motion, statistical concepts, such as spin diffusion,[1] proved to be useful in nuclear magnetic resonance, especially for solids with a large number of interacting spins. In many simple solid-state NMR experiments, the inclusion of a damping term is adequate for rationalizing experimental observations.[2] In this paper, we analyze situations where the deterministic character becomes apparent. Deterministic reversibility is put into evidence most clearly by echo experiments on solids with an extended network of dipolar coupled nuclear spins where the original state is recovered after an effective reversal of the preceding evolution.

Two related dipolar echo experiments have been described in the literature. The ''magic echo experiment,'' here called coherence echo experiment, introduced by Schneider and Schmiedel[3] and Rhim *et al.*,[4] refocuses the free induction decay (FID) under the influence of a secular dipolar Hamiltonian. The signal decay is caused by the transfer of single-spin coherence into unobservable multiple-spin coherence. It can be reconverted by the echo sequence into detectable single-spin coherence. This experiment loosely resembles the well-known Hahn echo experiment,[5] except that the refocused interaction is of a homogeneous nature in contrast to the Hahn echo experiment where it is inhomogeneous. Recently, Zhang *et al.*[6,7] described a closely related ''polarization echo experiment'' where an initial state evolves into multiple-spin order and is refocused back to the initial state of polarization by a suitable pulse sequence. This experiment produces the impression that a spin-diffusion process can be inverted by a sign change of the effective Hamiltonian. It implies that the system retains its memory and does not follow a statistical evolution.

In terms of practical applications of dipolar echo experiments in solids, it is conceivable to use them for the detection of random motional processes on the molecular level that destroy the spin memory and inhibit the echo formation. Molecular diffusion processes and intramolecular motion in the time range of micro- to milliseconds might be studied in this manner. An additional possibility is to exploit the intermediate build-up of multiple-spin order to infer the size of the involved spin clusters and to obtain information on the microscopic domain structure of solids.[8–11]

In order to improve the spectral resolution and sensitivity when applied to more complex solids, it is desirable to combine the dipolar echo experiments with magic angle spinning (MAS). However, magic angle spinning causes a partial averaging of the dipolar interactions and retards the dipolar evolution into multiple-spin order, rendering the experiment insensitive to dynamical and structural features. Hence, it is necessary to recover a strong effective dipolar Hamiltonian during the defocusing and refocusing periods of the echo experiment. The rotational averaging of the dipolar Hamiltonian could be defeated by spinning the sample at an

---

[a)] Present address: Materials Sciences Division, E. O. Lawrence Berkeley National Laboratory, 1 Cyclotron Road, and Chemistry Department, University of California, Berkeley, California 94720.

0021-9606/96/105(24)/10672/10/$10.00

angle different from the magic one during the defocusing and refocusing periods, while during the periods in which spectral resolution is required, the magic angle is chosen.[12]

In this article, we present an approach based on rotor-synchronized multiple-pulse sequences. The retrieval of the dipolar interaction is effected by the use of rotating frame/laboratory frame (R/L) pulse sequences.[13,14] By means of a simple modification it is possible to reverse the sign of the effective dipolar Hamiltonian and to induce the refocusing process. We compare the dipolar echoes under MAS with experiments performed under static conditions. In addition, we present possible schemes for monitoring the build-up of multiple-spin order that accompanies the dipolar evolution during the echo-formation process.

II. DIPOLAR ECHO EXPERIMENTS

The formation of dipolar echoes, after a preceding evolution for a time τ_1 under an average Hamiltonian $H_1^{(0)} = s_1 H$, can be induced by a sign change of the Hamiltonian to $H_2^{(0)} = s_2 H$, with $s_1 s_2 < 0$. Here, s_1 and s_2 are scaling factors and H the secular dipolar Hamiltonian. An echo occurs after the refocusing time

$$\tau_2 = |s_1|/|s_2|\tau_1 . \tag{1}$$

For all proton-resonance dipolar echo experiments, described in Secs. III and IV, the indirect excitation and detection scheme via carbon-13 resonance, suggested by Zhang *et al.*,[6] has been used. It allows for local injection and local observation of polarization or transverse magnetization at individual protons that are coupled to a rare carbon-13 spin. While for the observation of polarization echoes, this local observation scheme is mandatory,[6] it is optional for monitoring coherence echoes. The latter one could also be directly observed on the protons by a nonselective pulse sequence. However, in order to facilitate the comparison, the same indirect observation scheme is applied for all experiments.

The four pulse sequences used for polarization and coherence echoes in static and rotating solids, shown in Figs. 1 and 2, are all derived from the basic sequence of Fig. 1(a), proposed by Zhang *et al.*[6] In the course of the preparation period, the ^{13}C spins (S spins) are polarized by a Hartmann–Hahn transfer from the proton spins (I spins) during the time t_c. The remaining proton coherence decays during the following period t_s (see caption of Fig. 5). During the short second cross-polarization period t_d, the ^{13}C-bound protons (I_1 spins) are selectively repolarized, establishing the desired initial state with localized polarization. After the defocusing and refocusing periods τ_1 and τ_2, the proton polarization is transferred again to ^{13}C by a brief cross-polarization period t_d, followed by ^{13}C detection in the presence of proton decoupling.

While for experiments with static samples and for MAS spinning below 15 kHz a continuous-wave cross-polarization process is used, adiabatic passage Hartmann–Hahn cross polarization (APHH-CP) (Ref. 15) is applied for the magic-angle sample spinning experiments with $\omega_r/2\pi > 15$ kHz. APHH-CP using a passage through the first sideband of the Hartmann–Hahn matching condition leads to an improved cross-polarization efficiency.

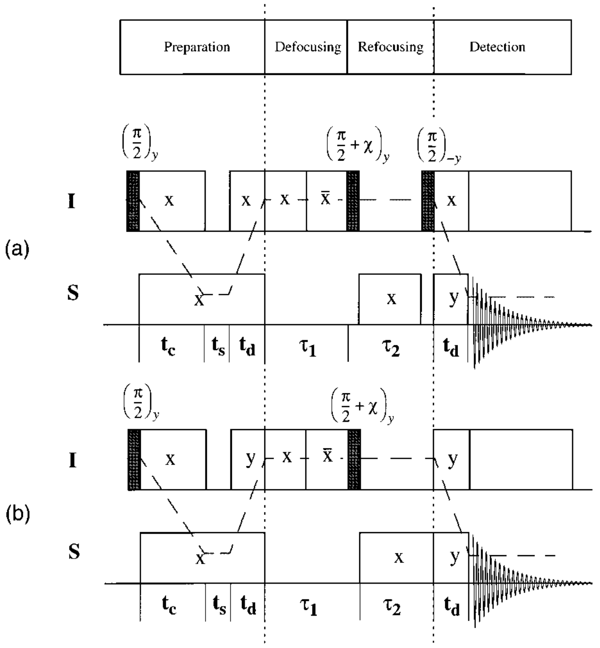

FIG. 1. Dipolar echo rf-pulse sequences for static solids. (a) Polarization echo sequence of Zhang *et al.* (Ref. 6) supplemented by a phase reversal of the rf field at time $\tau_1/2$ for the refocusing of rf field inhomogeneity. The preparation of the initial nonequilibrium polarization is accomplished by a two-way IS cross-polarization process. During the defocusing period an on-resonant rf spin-lock-field is applied. In the refocusing period, the I spins evolve freely in the external static magnetic field. A third IS cross-polarization step starts the detection period where the I-spin polarization is indirectly measured at the end of the refocusing period. The broken line shows the pathway of the relevant spin order. (b) Related coherence echo sequence. It differs from (a) merely by a $\pi/2$ rotation of the initial magnetization at the beginning of the defocusing period. The variable flip angle χ allows the monitoring of the emergence of multiple-quantum coherence at the end of the defocusing period τ_1, as explained in Sec. V. In standard echo experiments, χ is set equal to zero.

The same experimental schemes can be used for polarization echoes and for coherence echoes except for different initial conditions. Assuming a rf field applied with x polarization during the defocusing period τ_1, $\sigma(\tau_1=0)=I_{1x}$ is necessary for polarization echoes, Figs. 1(a) and 2(a), and $\sigma(\tau_1=0)=I_{1y}$ for coherence echoes, Figs. 1(b) and 2(b).

A. Dipolar echoes in static solids

The defocusing in static solids takes place during τ_1 in the rotating frame in the presence of a strong radio frequency field with the amplitude $\omega_1 \gg M_2^{1/2}$, applied along the x-axis (Fig. 1), where M_2 is the second moment of the proton resonance line, leading to a scaling factor $s_1 = -\frac{1}{2}$. The zero-order average dipolar Hamiltonian in the frame rotating with the rf frequency is then given by

$$\overline{H_1^{(0)}} = s_1 H_{xx} = -\tfrac{1}{2} \sum_{j<k} d_{jk}\, \tfrac{1}{2}\,(3\cos^2 \vartheta_{jk} - 1) \times (3 I_{jx} I_{kx} - \mathbf{I}_j \mathbf{I}_k), \tag{2}$$

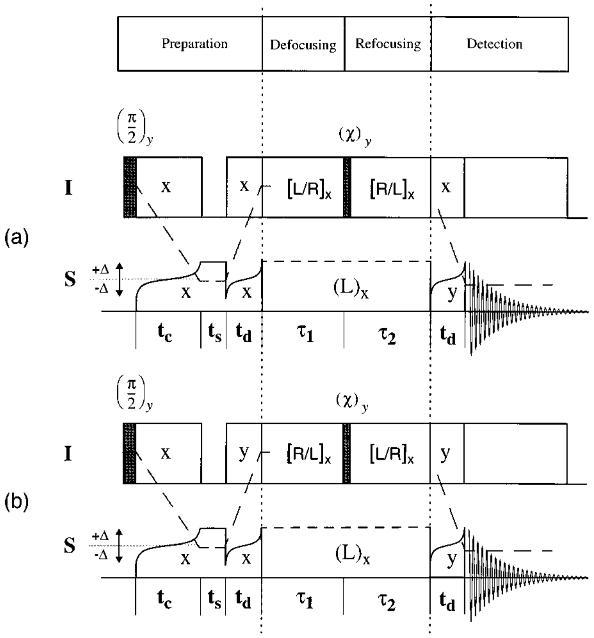

FIG. 2. Modified dipolar echo sequences designed for solids subjected to MAS. Preparation and detection periods are analogous to the static sequences except that all IS cross-polarization steps are performed with a more efficient tangential adiabatic passage through the Hartmann–Hahn matching condition (Ref. 15), suitable for high-speed MAS. During the defocusing and refocusing periods, multiple-pulse sequences (see Fig. 3) with a nonvanishing average secular dipolar Hamiltonian are applied. (a) Polarization echo experiment. (b) Coherence echo experiment. The optional pulse of variable flip angle χ_y has the same function as in Fig. 1 for monitoring the emerging multiple-quantum coherence. In standard echo experiments, χ_y is set equal to zero. During the laboratory frame L periods, S-spin decoupling $(L)_x$ is applied.

where the dipolar coupling constant, given in units of angular frequencies, is

$$d_{jk}=-\frac{\mu_0}{4\pi}\,\frac{\gamma_I^2\hbar}{r_{jk}^3}, \tag{3}$$

and where ϑ_{jk} denotes the angle of the internuclear vector $\mathbf{r}_{jk}$ of spins j and k with respect to the external static magnetic field. During the refocusing period τ_2, the unperturbed Hamiltonian with $s_2=1$ is active, bracketed by a pair of $(\pi/2)_{\pm y}$ pulses. This leads to the effective Hamiltonian

$$\overline{H_2^{(0)}}=s_2H_{xx}=\sum_{j<k} d_{jk}\ \tfrac{1}{2}\ (3\cos^2\ \vartheta_{jk}-1)(3I_{jx}I_{kx}-\mathbf{I}_j\mathbf{I}_k). \tag{4}$$

The effective Hamiltonians of Eqs. (2) and (4) have opposite signs and differ in their scaling by a factor 2. Hence, a dipolar echo occurs for $\tau_2=\frac{1}{2}\tau_1$. The proton chemical-shielding anisotropy is small compared to the proton dipolar interactions in calcium formate[16] and is neglected.

B. Dipolar echoes under MAS

For MAS conditions, the dipolar Hamiltonian becomes time-dependent and can be expressed as a Fourier series expansion,[17,18]

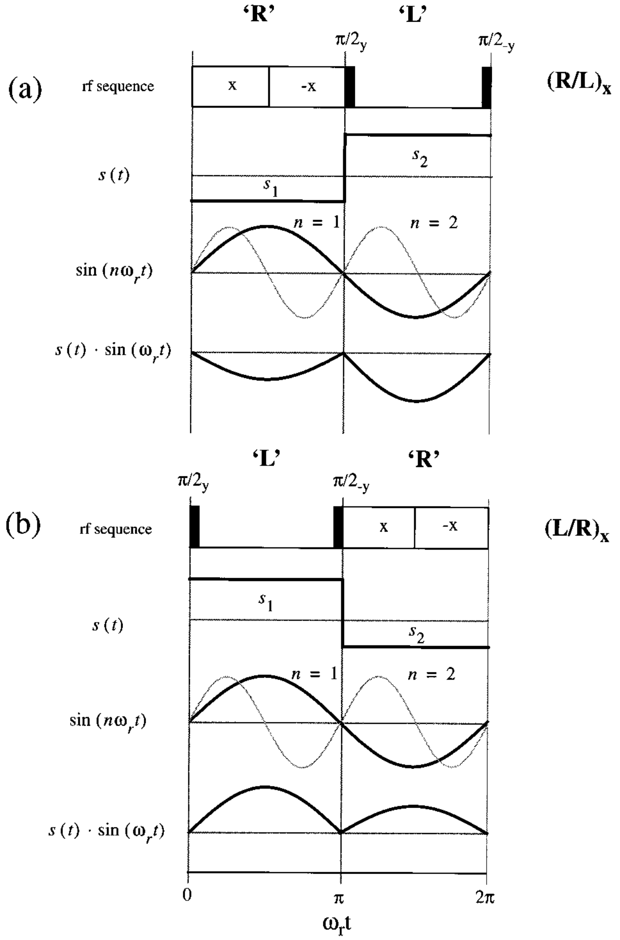

FIG. 3. Rotor-synchronized R/L and L/R pulse sequences for the dipolar recoupling in MAS experiments leading to dipolar Hamiltonians of opposite signs. The sign inversion of the ω_r-modulated term of the dipolar interaction is compensated by the scaling factor $s(t)$ of the alternating rotating frame (R) and laboratory frame (L) periods. The phase inversion of the rf field after a quarter rotation period leads to a refocusing of the evolution under the rf field and eliminates the effect of rf field inhomogeneities in zeroth order.

$$H(t)=\sum_{j<k}\sum_{n=-2}^{2} b_n^{jk}e^{in\omega_r t}(3I_{jx}I_{kx}-\mathbf{I}_j\mathbf{I}_k), \tag{5}$$

with the coefficients

$$b_0^{jk}=0,\ \ b_{\pm1}^{jk}=-d_{jk}/(2\sqrt{2})\sin 2\theta_{jk}e^{\pm i\varphi_{jk}}$$

and

$$b_{\pm2}^{jk}=\frac{d_{jk}}{4}\ \sin^2\ \theta_{jk}e^{\pm 2i\varphi_{jk}}. \tag{6}$$

θ_{jk} and φ_{jk} are the polar angles that orient the internuclear vector $\mathbf{r}_{jk}$ with respect to the MAS rotation axis and ω_r denotes the MAS angular frequency.

For rapid spinning $\omega_r \gg M_2^{1/2}$, the dipolar evolution is nearly quenched. It can be retrieved by the application of a rotating frame/laboratory frame (R/L) pulse sequence.[13,14] Its effect is visualized in Fig. 3(a). In close analogy to the dipolar echo experiment of Fig. 1, the dipolar evolution proceeds during the first half of the rotor cycle in the rotating frame with the Hamiltonian of Eq. (2) and during the second half in the laboratory frame with the Hamiltonian of Eq. (4). The time dependence, introduced by the sample rotation and given by Eq. (5), leads to a modulation by the first and second harmonics of ω_r. The sign change of the first harmonic is compensated, as shown in Fig. 3(a), by the sign change of the dipolar Hamiltonian, leading to a nonvanishing average dipolar Hamiltonian which, according to Ref. 14, is given in zero-order average Hamiltonian theory by

$$\overline{H_1^{(0)}}=\sum_{j<k}\zeta_{jk}(3I_{jx}I_{kx}-\mathbf{I}_j\mathbf{I}_k) \tag{7}$$

with

$$\zeta_{jk}=-\frac{3}{2\pi}\cdot\frac{d_{jk}}{\sqrt{2}}\sin(2\theta_{jk})\sin(\varphi_{jk}). \tag{8}$$

To construct an effective Hamiltonian with opposite sign, it is just necessary to interchange the R and L periods in Fig. 3(a), leading to the L/R sequence of Fig. 3(b) with the average Hamiltonian

$$\overline{H_2^{(0)}}=-\sum_{j<k}\zeta_{jk}(3I_{jx}I_{kx}-\mathbf{I}_j\mathbf{I}_k). \tag{9}$$

The echo experiments of Fig. 2 take advantage of these two pulse sequences. The angular dependence of the average Hamiltonians in Eqs. (7) and (9) is determined by the spherical harmonics $Y_{2\pm1}(\theta_{jk},\varphi_{jk})$, in contrast to the Hamiltonian for a static sample which depends on $Y_{20}(\vartheta_{jk})$. In principle, it is also possible to retrieve the Fourier coefficients with $n=\pm2$ in Eq. (5) by changing the direction of the quantization axis every quarter rotor cycle.

III. EXPERIMENT

The measurements were performed on homebuilt spectrometers at 300 K on a sample of polycrystalline calcium formate at a proton-resonance frequency of 220 MHz for the static experiments, and at 300 MHz for the MAS experiments. The accurate relative phase and the equality of the rf amplitudes for the four basic channels (0°,90°,180°,270°) are quite critical in these experiments. They were carefully adjusted on both spectrometers by means of tune-up sequences.[19] The sample was 5% ^{13}C-enriched and doped with 2% Cu(II) to shorten the proton T_1 relaxation time ($T_1=600\pm100$ ms) to allow for a faster sequence of experiments. The spin dynamics described in Secs. IV and V is by three orders of magnitude more rapid and not affected by the T_1 relaxation. At 300 K, calcium formate forms an orthorhombic crystal with two crystallographically inequivalent sites per unit cell.[20] The crystal structure consists of ''chains'' of Ca(II) ions alternating with pairs of O atoms. Formate ions bind the chains into a compact spatial network. The intricate proton–proton coupling network leads to a nearly Gaussian static proton NMR powder spectrum with a full-width at half-maximum of 17 kHz.[12]

Static polarization echo experiments were performed with the sequence (a) of Fig. 1, in some experiments with a π phase inversion of the spin locking rf field in the middle of the defocusing period τ_1 to refocus rf field inhomogeneities. The static coherence echo experiments used the sequence (b) of Fig. 1. The rf-field strengths on the two channels of the spectrometer were matched to $\omega_1/2\pi=100$ kHz for all static experiments.

Polarization and coherence echo experiments under MAS were performed with the sequences (a) and (b) of Fig. 2, respectively. The tangential adiabatic passage through the −1st sideband Hartmann–Hahn cross-polarization (APHH-CP) matching condition used a tangent depth $\Delta=0.5\omega_r/2\pi$ (in Hz). An overall increase in the IS polarization-transfer efficiency of 50%, in comparison to conventional Hartmann–Hahn cross polarization, has been achieved. Furthermore, the matching profile became less sensitive to amplifier instabilities. The proton rf-field strength was adjusted to $\omega_1/2\pi=125$ kHz for all MAS experiments. The MAS frequency was stabilized within 5 Hz using a homebuilt spinning speed controller. All MAS experiments were performed with a commercial 4 mm probe assembly (Chemagnetics).

Figure 4 shows polarization-decay and polarization-echo curves for calcium formate under MAS conditions, with spinning frequencies of 10.0, 13.3, and 16.6 kHz obtained with the pulse scheme displayed in Fig. 2(a). The sampling was performed at every full rotor period. For the echo experiments, a defocusing time of 300 μs was used. The contact time for the two brief cross-polarization transfers was adjusted to the first maximum of the transient oscillation[21] in the Hartmann–Hahn IS cross-polarization build-up ($t_d=80$ μs).

For comparison, polarization-decay and polarization-echo experiments under static conditions are shown in Figs. 5(a) and 5(b). The defocusing period τ_1 was set to 300 μs, and τ_2 was incremented from zero to 700 μs with $\Delta\tau_2=25$ μs. The contact time for the two brief cross-polarization steps of sequence A in Fig. 1 was adjusted to $t_d=60$ μs. For the echo experiment displayed in Fig. 5(a) a cw spin lock was used during τ_1 while for Fig. 5(b) the phase of the rf field was inverted at $\tau_1/2$ to eliminate possible effects of rf inhomogeneity.

IV. DISCUSSION OF THE EXPERIMENTAL POLARIZATION DECAY AND POLARIZATION ECHO CURVES

When comparing polarization decay and echo curves for static and rotating samples, it should be noted that for a static sample some proton polarization transfer occurs already during the preceding cross-polarization period t_d (Fig. 1) such that the polarization decay actually starts already at $\tau_1<0$. This is the reason why the polarization echo does not occur at the expected refocusing time $\tau_2=\tau_1/2$ but is delayed.[7] For the polarization decay under MAS in Fig. 4, the starting point of dipolar defocusing is better defined because the proton dipolar evolution during the cross-polarization time t_d is slowed down by the high-speed magic-angle spinning, provided that the rotation frequency exceeds the proton line-

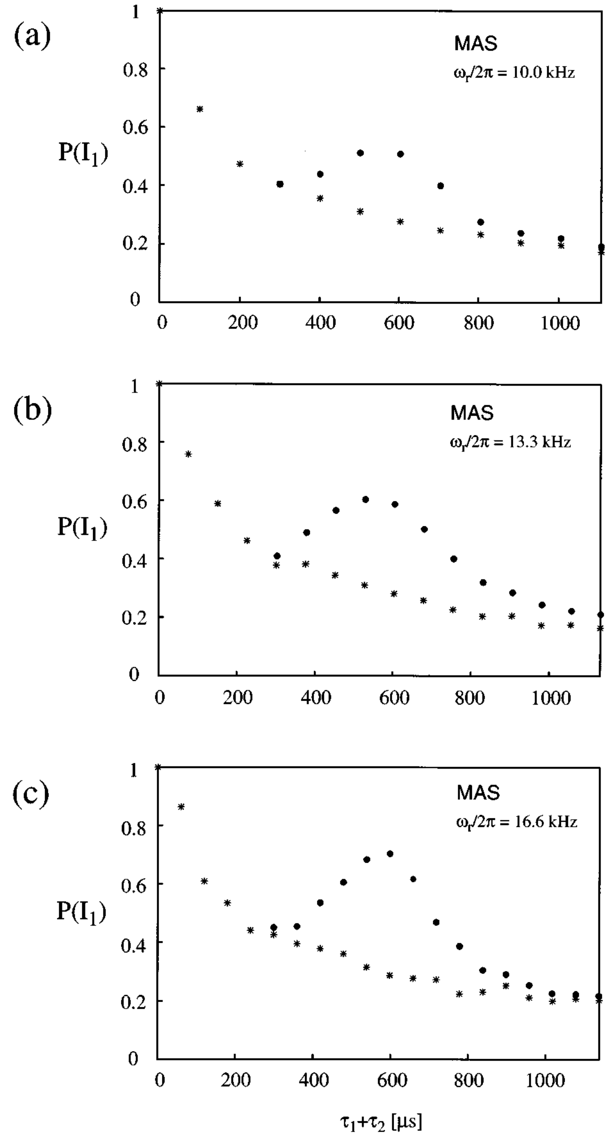

FIG. 4. Time evolution of the polarization $P(I_1)$ of the proton spins coupled to ^{13}C spins in a polycrystalline sample of calcium formate subjected to MAS. The MAS frequency is varied and is given in each graph. The experimental data is obtained with the pulse sequence (a) of Fig. 2 with $t_c=330$ μs, $t_s=2$ ms, $t_d=80$ μs, and $\omega_1/2\pi=125$ kHz. The results of two experiments are superimposed in each graph; asterisks result from experiments with $\tau_2=0$ and variable τ_1 (polarization decay). The filled circles represent the I-spin polarization for experiments with $\tau_1=300$ μs and variable τ_2 (polarization echo).

width under rf irradiation. Indeed, the polarization echoes in Fig. 4 occur, within experimental accuracy, at $\tau_2=\tau_1$.

Taking the above point into account, the polarization-decay curves for a spinning sample of calcium formate in Fig. 4 and for a static sample in Fig. 5 are remarkably similar. An initially rapid decay to about half amplitude in the first 100–200 μs is followed by a slower decay. Within the maximum measurement time of 1.2 ms, the expected quasi-equilibrium state with a polarization of $P(I_1)=0.05$, considering that 5% of all protons are polarized at time $\tau_1=0$, is not yet reached. It appears that there is no bottleneck for spin diffusion that would lead to a quasiequilibrium state at higher amplitude level as it was observed for ferrocene.[6,7,22]

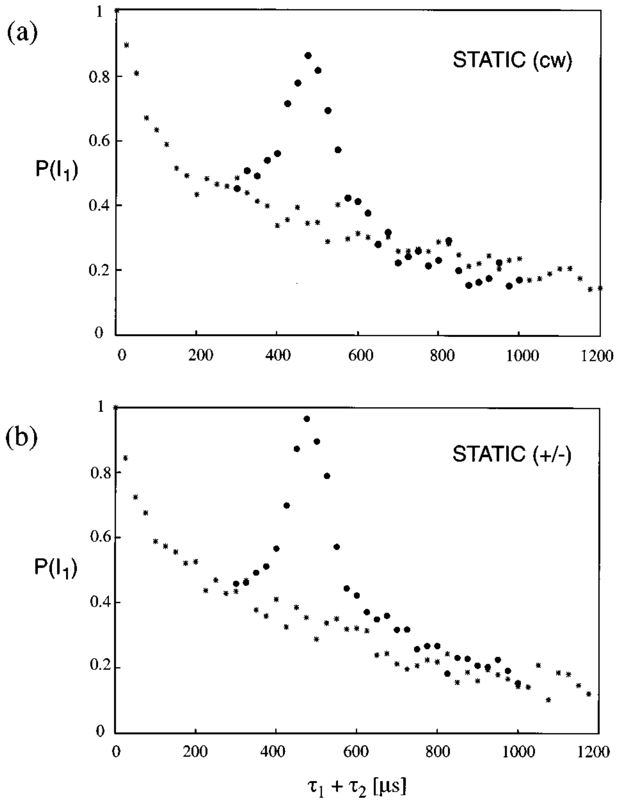

FIG. 5. Time evolution of the polarization $P(I_1)$ of the proton spins coupled to ^{13}C spins in a static polycrystalline sample of calcium formate obtained with pulse sequence A of Fig. 1 with $t_c=3$ ms, $t_s=0.5$ ms, $t_d=60$ μs, and $\omega_1/2\pi=100$ kHz. The measurements in (a) used an on-resonant cw spin lock during the evolution period. For the measurements in (b), the rf phase is inverted in the middle of the spin-lock period τ_1. As in Fig. 4, polarization decays and polarization echoes are superimposed in each graph. The delay time t_s was varied up to 20 ms in a second set of measurements (echo profiles not shown), using sequence A of Fig. 1 with $t_c=3$ ms, $t_d=60$ μs, $\omega_1/2\pi=100$ kHz, and $\tau_1=300$ μs ($t_s=0.5$ ms, 3.5 ms, 5.0 ms, 10.0 ms, and 20 ms), and show within experimental accuracy identical normalized polarization echo profiles. Hence, still existing proton multiple spin coherence after t_s has no measurable effect on the results discussed in Secs. IV and V.

From Fig. 5(b) it is apparent that for a static sample a pulse sequence compensated for rf field inhomogeneity (+/−) can efficiently refocus the polarization decay up to at least 500 μs defocusing time. For shorter echo times the echo amplitude can even surmount the initial amplitude by up to 10% (see e.g., Fig. 7). This is again an indication of dipolar defocusing already during the preceding cross-polarization period t_d. In Fig. 5(a) where the basic pulse sequence without sign inversion of the rf field at $\tau_1/2$ for compensation of rf field inhomogeneities is applied, a 15% intensity loss occurs under comparable conditions. Under MAS, a more severe loss in amplitude occurs that depends on the spinning speed.[12] It is apparent in Fig. 4 that the loss in echo amplitude decreases for more rapid spinning. But even at $\omega_r/2\pi=16.6$ kHz a 30% loss in echo amplitude occurs for a total dipolar evolution time of 600 μs. Nevertheless, the refocusing effect is clearly evident even for spinning at $\omega_r/2\pi=10$ kHz.

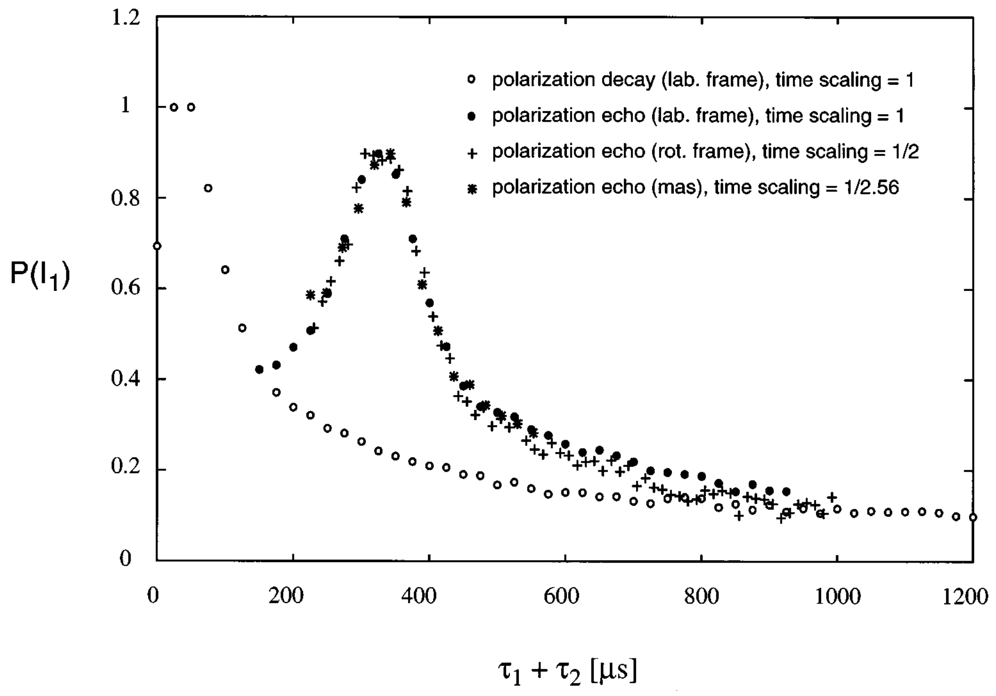

FIG. 6. Time evolution of the polarization $P(I_1)$ of the proton spins in a polycrystalline sample of calcium formate under static and MAS conditions. The laboratory-frame polarization decay (open circles) was measured using the pulse sequence shown in Fig. 1(a) with $\tau_1=0$, $t_c=3$ ms, $t_s=0.5$ ms, $t_d=60$ μs, and $\omega_1/2\pi=100$ kHz. τ_2 was incremented from zero to 1200 μs with $\Delta\tau_2=25$ μs. Initially the signal amplitude increases and leads to a polarization echo at $\tau_2\approx35$ μs. The refocusing is caused by the short cross-polarization time t_d. Three different normalized polarization-echo experiments are superimposed and time-scaled as indicated in the figure. (i) Laboratory-frame polarization echo (filled circles) obtained with the pulse sequence of Fig. 1(a) with $t_c=3$ ms, $t_s=0.5$ ms, $t_d=60$ μs, $\tau_1=300$ μs, and $\omega_1/2\pi=100$ kHz. (ii) Rotating-frame polarization echo (crosses) obtained with the reverse arrangement of the defocusing and refocusing periods of Fig. 1(a) ($t_c=3$ ms, $t_s=0.5$ ms, $t_d=60$ μs, $\tau_1=150$ μs, and $\omega_1/2\pi=124$ kHz). (iii) MAS polarization echo at $\omega_r/2\pi=16$ kHz (asterisks) obtained with the same experimental parameters as described in the caption of Fig. 4.

The different widths of the polarization echoes for static and rotating samples can be understood by the different angular factors $\zeta_{jk}(\vartheta_{jk})=\frac{1}{2}(3\cos^2\vartheta_{jk}-1)$ of Eq. (4) and $\zeta_{jk}(\theta_{jk},\varphi_{jk})$ of Eq. (8). For a powder sample, the angular factors are inhomogeneously distributed and lead to an inhomogeneous echo peak shape. However, the insensitivity of the peak shape on the detailed dipolar coupling network justifies the computation of average angular factors. Because the contributions of the different interactions to the second moment are additive, we average the squares of ζ_{jk} and obtain

$$\overline{\zeta^2_{\rm static}}=\frac{1}{4\pi}\int_0^\pi\int_0^{2\pi}\left[\frac{1}{2}(3\cos^2\vartheta-1)\right]^2\sin\vartheta d\vartheta d\varphi =\frac{1}{5}, \tag{10}$$

$$\overline{\zeta^2_{\rm mas}}=\frac{1}{4\pi}\int_0^\pi\int_0^{2\pi}\left[\frac{3}{2\pi\sqrt{2}}\sin 2\theta\sin\varphi\right]^2\sin\theta d\theta d\varphi =\frac{3}{10\pi^2}. \tag{11}$$

For the ratio of the echo peakwidths, one finds

$$\frac{\Delta_\tau^{\rm mas}}{\Delta_\tau^{\rm static}}=(\overline{\zeta^2_{\rm static}}/\overline{\zeta^2_{\rm mas}})^{1/2}=2.56. \tag{12}$$

An experimental verification of this scaling factor is given in Fig. 6. It shows the polarization decay (open circles) as well as a series of superimposed polarization echoes for static and MAS conditions. The polarization decay was measured in the laboratory frame with the sequence (a) of Fig. 1 with $\tau_1=0$ and τ_2 incremented from zero to 1200 μs with $\Delta\tau_2=25$ μs. Due to the preceding cross-polarization time τ_d the signal amplitude initially increases leading to an echo at $\tau_{\rm echo}\approx35$ μs. The laboratory-frame polarization echo (filled circles), recorded with the sequence (a) of Fig. 1 with $\tau_1=300$ μs, is normalized for $\tau_2=0$ with respect to the polarization decay at the nominal laboratory-frame defocusing time of $\tau_1=150$ μs. Two additional normalized polarization echoes are superimposed and time-scaled; a rotating-frame polarization echo (crosses) was recorded with the reverse arrangement of the rotating-frame and laboratory-frame periods of the pulse scheme (a) of Fig. 1, with $\tau_1=150$ μs. Here a time-scaling factor of 1/2 has to be applied because the echo occurs in the presence of a spin-locking rf field. Similarly, the MAS polarization echo of Fig. 4(c) is plotted with a time-scaling factor of 1/2.56 (asterisks). It is evident

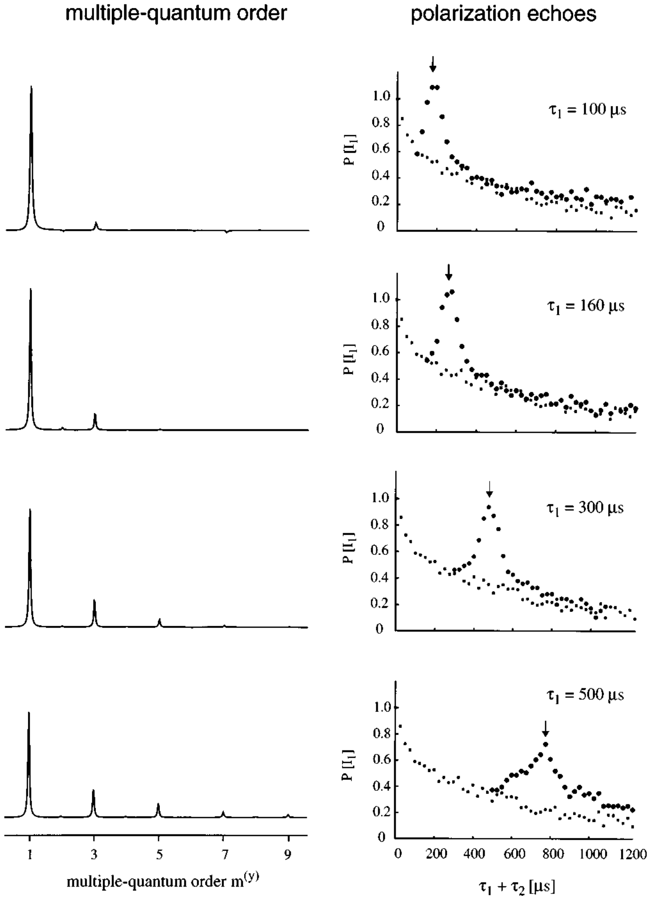

FIG. 7. Observed ^{1}H multiple-quantum order of static calcium formate as a function of the defocusing time τ_1 recorded at a proton resonance frequency of 220 MHz. The spectra are obtained with the polarization-echo-detected experiment of Fig. 1(a) with a π-phase inversion at $\tau_1/2$ and $t_c=3$ ms, $t_s=0.5$ ms, $t_d=60$ μs, and $\omega_1/2\pi=100$ kHz. For each spectrum, the corresponding polarization decay and polarization echo are displayed for reference.

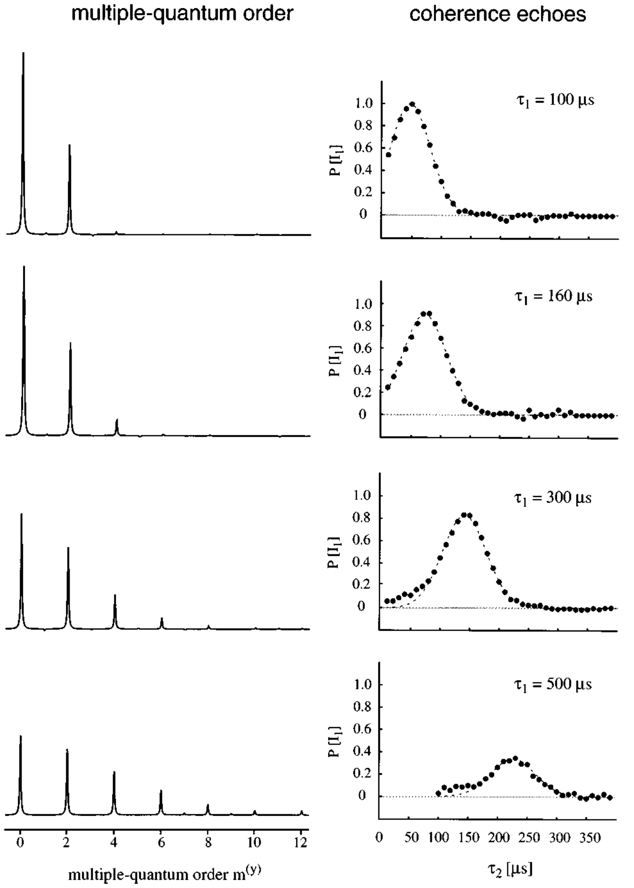

FIG. 8. Observed ^{1}H multiple-quantum order spectra of static calcium formate taken at a proton resonance frequency of 220 MHz for a static sample with different coherence defocusing times τ_1. The coherence-echo experiment of Fig. 1(b) was used for the detection of even-order multiple-quantum modes. For each spectrum the corresponding coherence echo is displayed for reference. The echo peak shapes have been fitted by a Gaussian $\{\langle I_{1x}(\tau_2)\rangle=\exp[-0.5M_{2,\mathrm{exp}}(\tau_2-\tau_{\mathrm{echo}})^2]$, broken lines$\}$. We obtain $M_{2,\mathrm{exp}}=(8.4\pm0.4)\times10^8\ \mathrm{s}^{-2}$. The same experimental conditions as described in Fig. 7 were used.

that within experimental accuracy the build-up and decay of the various polarization echo profiles can be explained by the scaling law of Eq. (12).

V. CREATION AND DETECTION OF MULTIPLE-SPIN ORDER IN THE POLARIZATION AND COHERENCE DECAY

The polarization or coherence decay in an extended dipolar coupled spin system is caused by the development of multiple-spin modes which are not directly observable. The monitoring of the build-up of multiple-spin order is of considerable interest, as it might provide insight into the dynamics associated with the defocusing and the refocusing of spin order in the context of echo formation. Moreover, the time development of multiple-spin modes reflects properties of the dipolar coupling network. The extent of local spin clustering in disordered materials, for example, can be studied in this way.[9–11]

In this context it is necessary to carefully distinguish between multiple-spin order and multiple-quantum coherence. The degree of multiple-spin order is measured by the number of spins involved in a product term contained in the density operator. Terms such as $I_1^+I_2^+I_{3z}$ and $I_{1z}I_{2z}I_{3z}$, for example, represent three-spin order. The degree of multiple-spin order is independent of the reference frame and is reduced to a mere counting of individual spins.

The degree of multiple-quantum coherence or multiple-quantum order, on the other hand, is related to a selected quantization axis u, and is characterized by the membership to an irreducible representation of the one-dimensional rotation group about the selected axis, expressed in terms of a magnetic quantum number $m^{(u)}$.[23] An operator term A represents $m^{(u)}$ quantum coherence with respect to the quantization axis u when A shows the transformation behavior

$$\exp(-i\chi F_u)A\ \exp(i\chi F_u)=A\ \exp[-im^{(u)}\chi], \qquad (13)$$

where F_u is the total angular momentum operator component along the direction u and χ the rotation angle about this axis. Thus with respect to z as quantization axis, the term $I_1^+I_2^+I_{3z}$ represents $m^{(z)}=2$ quantum coherence while $I_{1z}I_{2z}I_{3z}$ represents $m^{(z)}=0$ quantum spin order. On the other hand, with respect to the y axis, $I_1^+ I_2^+ I_{3z}$ is a linear contribution of $m^{(y)}=0,\pm 1,\pm 2,\pm 3$ quantum coherence, while $I_{1z}I_{2z}I_{3z}$ contains $m^{(y)}=\pm 1$ and ± 3 quantum coherence.

In the following, we investigate the extent of multiple-quantum coherence at the end of the defocusing period τ_1, at which point the maximum degree of multiple-quantum coherence exists, and we select the y axis as the relevant quantization axis. The different orders can be separated by a systematic variation of the pulse rotation angle $0 \leq \chi \leq 2\pi$ in Fig. 1 and Fig. 2 in a set of successive experiments and by a Fourier transformation with respect to χ for a sufficiently dense set of sampling points in χ space.

The multiple-quantum orders that can be reached in the defocusing period τ_1 depend on the initial conditions. The defocusing is caused by the truncated dipolar Hamiltonian of Eq. (7) which can be written in a form adapted to the y-quantization axis,

$$\overline{H_1^{(0)}} = \sum_{j<k} \zeta_{jk}\Big[-I_{jy}I_{ky} + \tfrac{1}{2}(I_{jx}I_{kx}+I_{jz}I_{kz}) + \tfrac{3}{2}(I_{jx}I_{kx}-I_{jz}I_{kz})\Big], \tag{14}$$

where the three terms are of multiple-quantum orders $m^{(y)}=0$, 0, and ± 2, respectively. For a polarization echo experiment, the initial condition $\sigma(\tau_1=0)=I_{1x}$ is of order $m^{(y)}=\pm 1$ and can evolve under the dipolar Hamiltonian exclusively into odd higher orders. On the other hand, for a coherence echo experiment with the initial condition $\sigma(\tau_1=0)=I_{1y}$, which is of order $m^{(y)}=0$, only even orders can be created during the defocusing period, when the evolution under the rf field, applied along the x axis, is refocused by a phase inversion at the time $\tau_1/2$.

Experimental $m^{(y)}$ multiple-quantum spectra, obtained with the static polarization echo sequence, are shown in Fig. 7 for a sample of calcium formate powder. The corresponding polarization decays with superimposed polarization echoes are shown also. The experiments have been performed according to the scheme of Fig. 1(a). The flip angle χ was incremented in steps of $\Delta\chi = \pi/m_{\max}^{(y)}$ from $-\pi$ to $+\pi$, where $m_{\max}^{(y)}$ is the maximum order to be observed. The measured signals were stored as a two-dimensional data matrix and Fourier-transformed with respect to χ. The duration τ_1 of the defocusing period is indicated on the spectra in Fig. 7. The duration of the laboratory frame refocusing period τ_2 was chosen to maximize the echo intensity. The creation of the higher quantum orders with increasing defocusing time is evident. For short defocusing periods ($\tau_1=100$–$160\ \mu$s), the intensity of the $m^{(y)}$ 3-quantum order is dominant. For longer τ_1, higher orders up to $m^{(y)}=9$ are excited.

Related spectra obtained with the coherence-echo detection scheme of Fig. 1(b) for a static sample are displayed in Fig. 8. The corresponding spectra for MAS conditions ($\omega_r/2\pi=16$ kHz) with the scheme of Fig. 2(b) using the R/L (L/R) recoupling sequences are displayed in Fig. 9. Again, at short defocusing times the $m^{(y)}=2$ quantum order is dominant which is progressively converted into higher spin orders with increasing τ_1. We note that in the MAS experiments, the higher quantum modes are emerging more slowly than for the static measurements.

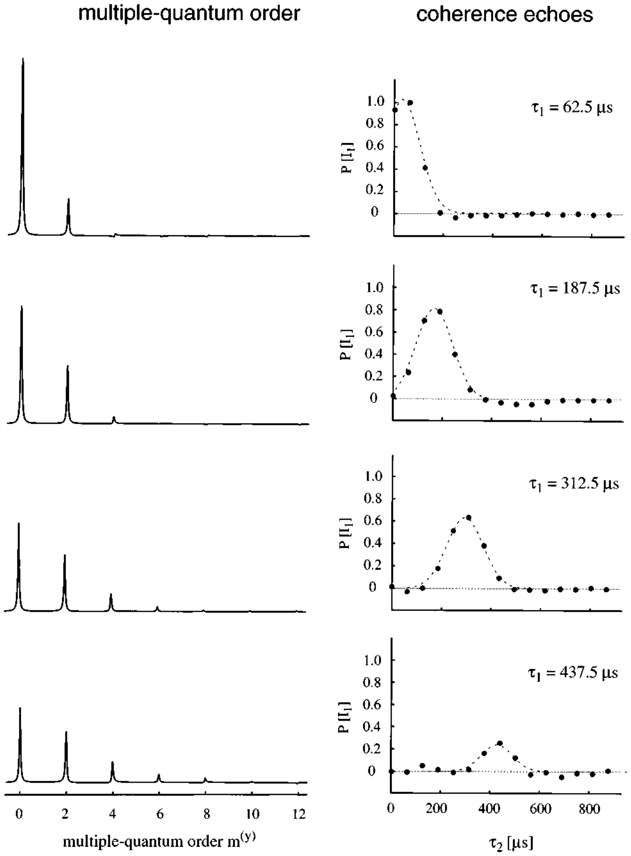

FIG. 9. Observed ^{1}H multiple-spin order spectra of calcium formate under MAS with different coherence defocusing periods taken at a proton resonance frequency of 300 MHz. The coherence echo experiment of Fig. 2(b) was used for the detection of even-order multiple-quantum coherence. For each spectrum the corresponding coherence echo is displayed for reference. The MAS frequency was 16 kHz, $t_c=300\ \mu$s, $t_s=2$ ms, $t_d=90\ \mu$s and $\omega_1/2\pi=125$ kHz. Sampling was performed at every full rotor cycle. The echo peak shapes have been fitted by a Gaussian (broken lines). We obtain for the MAS case $M_{2,\mathrm{exp}}=(1.7\pm 0.3)\times 10^8\ \mathrm{s}^{-2}$.

The build-up of multiple quantum order in dipolar coupled spin systems has created much interest in the past, both on the experimental[8–10,23] as well as on the theoretical[11,24,25] side. Its comprehension can deliver useful information on solid-state structures, particularly on clustered spin domains, and can critically test model concepts of many-body interactions. The most comprehensive experimental material stems from Baum, Pines, and co-workers[9,10] and from Levy *et al.*[25] Theoretical models have been developed by Munowitz *et al.*[24] and more recently in the extensive and thorough work by Lacelle[11] who critically reviews the various concepts. From this work no generally applicable universal model resulted. It seems that the resulting distributions of multiple quantum coherence and the corresponding build-up rates are influenced by system-specific parameters, and possibly also by the measurement strategies.

Figure 10 presents logarithmic plots of the observed $m^{(y)}$ multiple quantum intensities measured on calcium formate

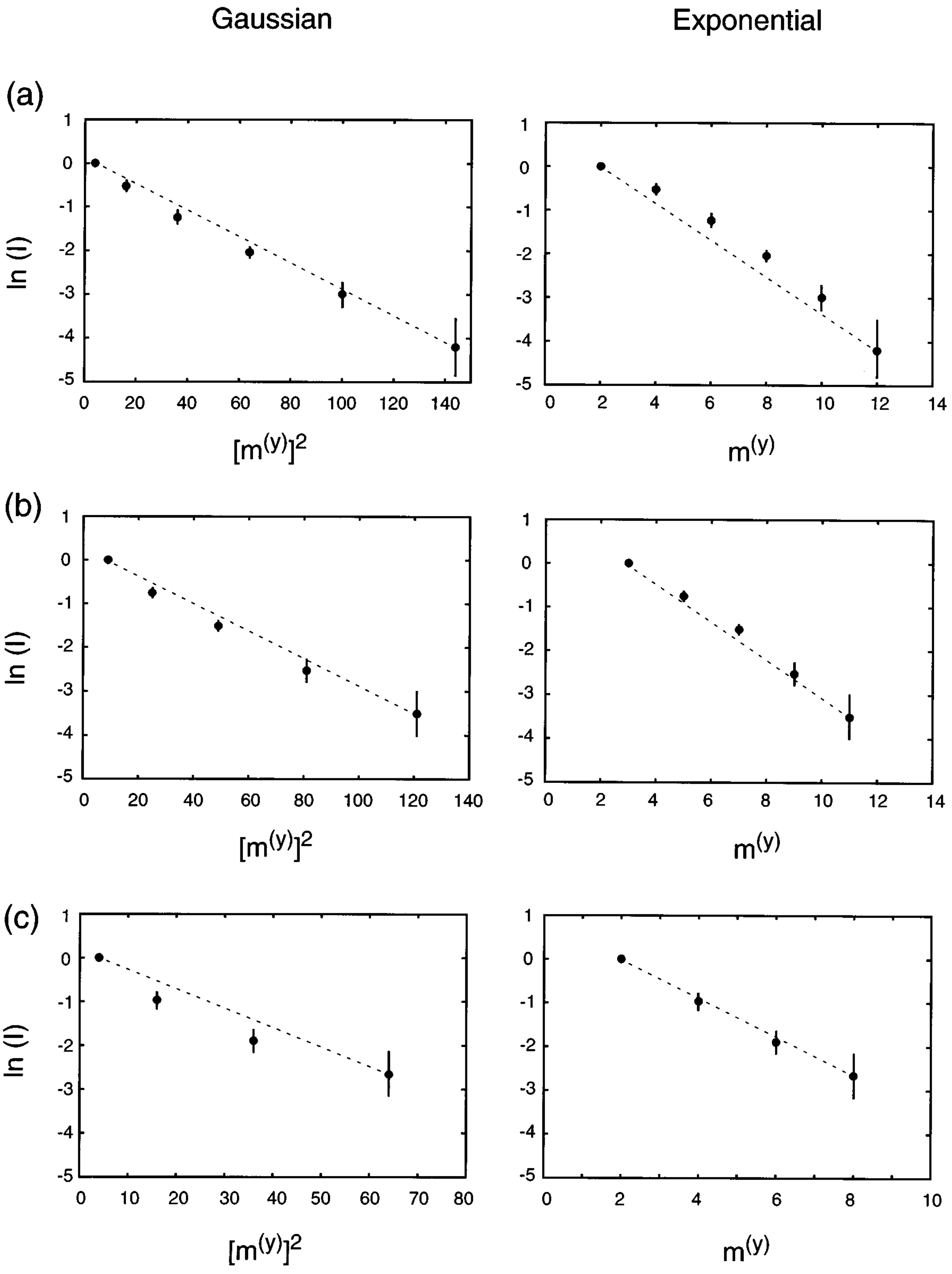

FIG. 10. Logarithm of the intensity profile $I[m^{(y)}]$ as a function of $[m^{(y)}]^2$ (left frames) and $m^{(y)}$ (right frames). (a) Static coherence echo experiments with τ_1=500 μs. (b) Static polarization echo experiments with τ_1=500 μs. In both cases (a) and (b) the points represent the average over two independent measurements. (c) MAS coherence echo experiments with τ_1=437.5 μs. The straight lines are guides to the eye.

for coherence and polarization echoes in static and rotating samples. The logarithm of the intensity is plotted vs the quantum number $m^{(y)}$ and its square $[m^{(y)}]^2$. For an exponential distribution function,[27] a linear plot against $m^{(y)}$ is expected while for a Gaussian (statistical) distribution[9,10,24–26] of the multiple quantum intensities a linear plot against $[m^{(y)}]^2$ would result. It is apparent that the data reflect intermediate situations between these two cases.

It appears to us premature to rationalize these data in terms of a specific model concept. More systematic data would have to be collected on different molecular systems to allow for general conclusions on the build-up of multiple spin order.

VI. CONCLUSIONS

Novel echo experiments under MAS conditions have been described. A recoupling technique, based on a R/L sequence, allows one to recover the dipolar interactions that are averaged normally to zero by MAS, and to refocus the induced evolution by a reversed recoupling sequence with a L/R sequence that produces a dipolar Hamiltonian of opposite sign. The echo experiments, which have been applied in this paper to strongly coupled proton systems, can also be used for spin systems with weak couplings and large chemical shifts, such as ^{13}C and ^{15}N. For the compensation of the large chemical shifts, it is advisable to use the offset-compensated RIL sequence[14] together with the complementary LIR sequence. An alternative approach for the creation of rotational resonance echoes in ^{13}C spin systems has recently been presented by Karlsson *et al.*[28]

A procedure has been applied that allows the monitoring of the build-up of multiple-quantum order in the course of a polarization- or coherence-decay experiment. It is applied to polarization- and coherence-echo experiments in static and rotating samples of calcium formate.

Dipolar echo experiments, in general, can be used to monitor motional processes in solids. They may lead to an attenuation of the echo amplitude which depends on the rate and the kind of process. Echo experiments under magic-angle sample spinning conditions have the additional advantage to separate, in a two- or three-dimensional fashion, the various spectral components according to their isotropic chemical shifts. Such experiments have the inherent potential to be applied also to complex systems with numerous inequivalent sites.

ACKNOWLEDGMENTS

We are indebted to Professor Ulrich W. Suter for his help and support. We would also like to thank Dr. Matthias Ernst, Dr. Marc Baldus, and Professor Beat H. Meier (University of Nijmegen, The Netherlands) for helpful discussions and Paul Signer (ETHZ) and Josef Eisenegger (ETHZ) for excellent technical assistance. This work has been supported by the Swiss National Science Foundation. We would like to acknowledge the revealing comments by an unknown referee.

[1] N. Bloembergen, Physica (Utrecht) **15**, 386 (1949).
[2] A. Abragam, *The Principle of Nuclear Magnetism* (Clarendon, Oxford, 1961).
[3] H. Schneider and H. Schmiedel, Phys. Lett. **30A**, 298 (1969).
[4] W. K. Rhim, A. Pines, and J. S. Waugh, Phys. Rev. Lett. **25**, 218 (1970); Phys. Rev. B **3**, 684 (1971).
[5] E. L. Hahn, Phys. Rev. **80**, 580 (1950).
[6] S. Zhang, B. H. Meier, and R. R. Ernst, Phys. Rev. Lett. **69**, 2149 (1992).
[7] S. Zhang, B. H. Meier, and R. R. Ernst, Solid State Nucl. Magn. Reson. **1**, 313 (1992).
[8] Y. S. Yen and A. Pines, J. Chem. Phys. **78**, 3579 (1983).
[9] J. Baum and A. Pines, J. Am. Chem. Soc. **108**, 7447 (1986).
[10] J. Baum, M. Munowitz, A. N. Garroway, and A. Pines, J. Chem. Phys. **83**, 2015 (1985).
[11] S. Lacelle, Adv. Magn. Opt. Res. **16**, 173 (1991).
[12] M. Tomaselli, Ph.D. thesis No. 11455, ETH Zürich, 1996.
[13] T. Fujiwara, A. Ramaamoorthy, K. Nagayama, K. Hioka, and T. Fujito, Chem. Phys. Lett. **212**, 389 (1993).
[14] M. Baldus, M. Tomaselli, B. H. Meier, and R. R. Ernst, Chem. Phys. Lett. **230**, 329 (1994); M. Baldus, B. H. Meier, M. Tomaselli, and R. R. Ernst, presented at the Experimental NMR Conference 36th, Boston, April, 1995 (unpublished).
[15] S. Hediger, B. H. Meier, and R. R. Ernst, Chem. Phys. Lett. **240**, 449 (1995).
[16] U. Haeberlen, *Advances in Magnetic Resonance, Suppl. 1 High Resolution NMR in Solids* (Academic, New York, 1976).
[17] M. M. Maricq and J. S. Waugh, J. Chem. Phys. **70**, 3300 (1979).
[18] M. Mehring, *High Resolution NMR in Solids* (Springer, Heidelberg, 1983).
[19] D. P. Burum, M. Linder, and R. R. Ernst, J. Magn. Reson. **43**, 463 (1981).
[20] N. Burger and H. Fuess, Acta Crystallogr. B **33**, 1968 (1977).
[21] L. Müller, A. Kumar, T. Baumann, and R. R. Ernst, Phys. Rev. Lett. **32**, 1402 (1974).
[22] H. M. Pastawski, P. R. Levstein, and G. Usaj, Phys. Rev. Lett. **75**, 4310 (1995).
[23] D. Suter and J. G. Pearson, Chem. Phys. Lett. **144**, 328 (1988).
[24] M. Munowitz, A. Pines, and M. Mehring, J. Chem. Phys. **86**, 3172 (1987); M. Munowitz and M. Mehring, Chem. Phys. **116**, 79 (1987).
[25] D. H. Levy and K. K. Gleason, J. Phys. Chem. **96**, 8125 (1992).
[26] B. E. Scruggs and K. K. Gleason, J. Magn. Reson. **99**, 149 (1992).
[27] S. Lacelle, S.-J. Hwang, and B. C. Gerstein, J. Chem. Phys. **99**, 8407 (1993).
[28] T. Karlsson, M. Helmle, N. D. Kurur, and M. H. Levitt, Chem. Phys. Lett. **247**, 534 (1995).